Bleed Effects on Shock/Boundary-Layer Interactions in Supersonic Mixed Compression Inlets

M.K. Fukuda,*
Case Western Reserve University, Cleveland, Ohio

W.R. Hingst†
NASA Lewis Research Center, Cleveland, Ohio

and

E. Reshotko‡
Case Western Reserve University, Cleveland, Ohio

An experimental investigation has been conducted to determine the effect of bleed region geometry and bleed rate on the boundary layer after a shock-wave/boundary-layer interaction in an axisymmetric, mixed compression inlet at $M_\infty = 2.5$. The full realizable reduction in transformed form factor, H_{tr}, is obtained by bleeding off about half the incident boundary-layer mass flow. Bleeding upstream or downstream of the interaction region results in much lower values of H_{tr} than bleeding across the interaction region. Slanted holes are found to be more effective than normal holes in the single comparison made. Two different bleed hole sizes were tested without significant difference in performance.

Nomenclature

AS = across-the-shock bleed configuration
DS = downstream-of-shock bleed configuration
H_c = compressible form factor (δ^*/θ)
H_{tr} = transformed form factor, $\{H_c - [(\gamma-1)/2]M_e^2\}/\{(T_w/T_o)[1+((\gamma-1)/2)M_e^2]\}$
LN = large normal bleed holes
M_e = boundary-layer edge Mach number
M_∞ = freestream Mach number
$\dot{m}_1$ = nondimensional forward centerbody bleed mass flow
$\dot{m}_5$ = nondimensional cowl bleed mass flow
p = static pressure
p_o = freestream stagnation pressure
scoop = scoop bleed configuration
slant = slanted bleed holes
SN = small normal bleed holes
R_c = cowl lip radius
T_o = total temperature
T_w = wall temperature
US = upstream-of-shock bleed configuration
x = axial distance from centerbody tip
y = distance normal to surface
γ = ratio of specific heats
δ^* = compressible displacement thickness
θ = compressible momentum thickness

Introduction

THE growth of boundary layers, primarily turbulent, on the internal surfaces of supersonic inlets may play a major role in the overall performance of such inlets. Several of the ways in which boundary layers influence inlet performance are through the modification of the external flow field due to decreasing the amount of inviscid flow area, the forward shifting of the shock structure, and possibly, the separation of the boundary layer which may cause inlet unstart.

Boundary-layer separation is usually associated with adverse pressure gradients and/or shock/boundary-layer interactions which are necessarily present in mixed compression supersonic inlets. Thus the characteristics of boundary-layer growth on the internal surfaces of a supersonic inlet may cause changes, sometimes very drastic ones, in the performance of such an inlet.

To control the growth of the boundary layer on the internal surfaces of an inlet, a system of bleeding the boundary layer at various locations may be incorporated into the inlet. The bleed system usually removes the low-momentum portion of the boundary layer through porous sections, slots, or scoops. In this way, the size and characteristics of the boundary layer are somewhat controlled.

A penalty is incurred, however, in maintaining a nonseparating boundary layer by bleeding. The bleed mass flow is not usually reinjected into the inlet, so part of the captured mass flow is lost. To compensate for this loss in mass flow, a larger nacelle may be needed which would increase the friction drag and inlet weight. In addition, the bleed flow is usually vented overboard through bleed exits, a phenomenon which also incurs a drag penalty. Thus it is desirable to minimize the amount of boundary-layer bleed, while still providing good internal aerodynamic performance.

Experiments incorporating bleed systems in a supersonic inlet have been performed previously,[1-3] and there have also been studies[4-5] on shock-wave/boundary-layer interactions with and without bleed in simpler geometries. There has been a study[6] on the effect of bleed for a given geometry and the effect of bleed system geometry on the bleed mass flow. These types of information have ultimately been used to design supersonic inlets to obtain optimum performance.[7-8]

The purpose of this experiment[9] was to further investigate the effects of bleed region geometry and bleed mass flow rate on the characteristics of a turbulent boundary layer after a shock-wave/boundary-layer interaction in a supersonic inlet.

Presented as Paper 75-1182 at the AIAA/SAE 11th Propulsion Conference, Anaheim, Calif, Sept. 29-Oct 1, 1975; submitted Dec. 19, 1975; revision received June 10, 1976.

Index categories: Boundary Layers and Convective Heat Transfer-Turbulent; Airbreathing Propulsion, Subsonic and Supersonic.

*Graduate Research Assistant. Student Member AIAA.

†Aerospace Engineer.

‡Professor of Engineering. Fellow AIAA.

With this aim, several types of bleed configurations were studied. These configurations included variation of bleed hole size, angle of bleed hole to the surface normal, and bleed hole pattern. In addition to the porous or discrete-hole-type bleed, an axisymmetric scoop was also used. Each of the configurations was tested over a range of bleed mass flow rates.

In order to best reproduce the Mach number and pressure variations encountered in mixed compression inlets, as well as to study the effects of bleed on successive shock/boundary-layer interactions, the study was conducted on an actual inlet tested in the NASA Lewis Research Center 10×10 ft supersonic wind tunnel at a freestream Mach number of 2.50. The supersonic inlet used for this experiment was a mixed compression axisymmetric inlet having a design Mach number of 2.50 and with 60% of the supersonic area contraction occurring internally. The inlet was operated with a cold-pipe choked plug assembly instead of an engine. It was basically the same inlet used in the previously cited studies[1-2] with the exception of new external cowl pieces to control bleed mass flow rate and a bleed region in place of a solid wall in the first centerbody shock/boundary-layer interaction region.

Apparatus and Procedure

Inlet Geometry

The axisymmetric mixed compression inlet with a design Mach number of 2.50 that was used in this study is shown schematically in Fig. 1. At the design condition, 40% of the supersonic area contraction is external and 60% is internal. The inlet has a capture radius, R_c, of the 23.65 cm and a capture area of 1757 cm^2. The inlet was tested with a cold-pipe choked-plug assembly in place of an engine.

The external compression was accomplished with a 12.5° half-angle cone which remained conical to inlet station, x/R_c, of 2.88 where x is the axial distance from the spike tip. The cowl lip began at an x/R_c location of 2.01 with an internal lip angle of 0°. At the design condition, the geometric throat, which was 5.75 cm across the annulus, was at an x/R_c location of 3.48 and the compressor face was located an an x/R_c location of 7.72. The centerbody was supported by three equally spaced struts which were also used to duct the centerbody bleed flow overboard.

Shock Locations

The cowling of the inlet produced an internal shock wave which reflected first off the centerbody, then off the cowl, reaching the throat region for a second centerbody reflection. In critical mode operation the second centerbody reflected shock was the terminal shock, while in supercritical operation a second cowl reflection occurred and the terminal shock was held downstream of the geometric throat. The shock reflection points, calculated by the method of Ref. 10, were at x/R_c locations of 2.88 and 3.48 on the centerbody and 3.25 on the cowl. Improved computations of shock reflection points, taking δ^* effects into account, were made by the method of Refs. 11, 12, and 13. The shock reflection points obtained from these calculations, termed the δ^*-added impingement points, were at x/R_c locations of 2.84 and 3.43 on the centerbody and 3.20 on the cowl. A comparison of the two calculations is presented schematically in Fig. 2. This comparison shows that the effect of the internal boundary layers is to shift the entire shock structure slightly forward.

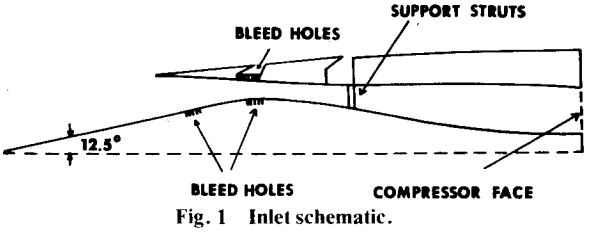

Fig. 1 Inlet schematic.

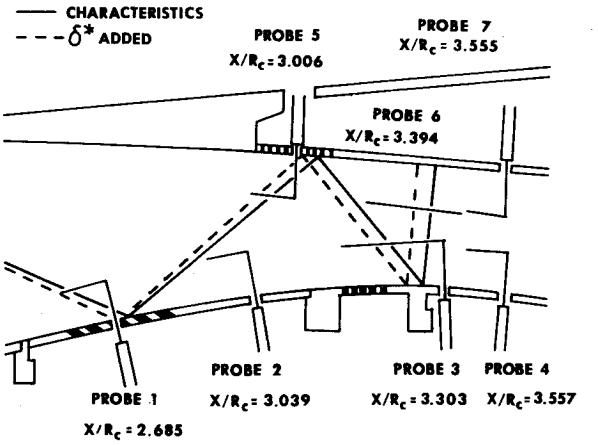

Fig. 2 Comparison of method of characteristics and δ^*-added shock impingement locations: a) centerbody; b) cowl.

Bleed System

The behavior of the boundary layer after a shock/boundary-layer interaction was studied under varying bleed conditions and bleed region configurations. The types of bleed sections used were porous bleed, consisting of rows of holes, and an axisymmetric scoop. Interchangeable bleed sections were placed in the forward cowl and centerbody around the shock/boundary-layer interaction regions. Bleed was also incorporated in the aft centerbody region just ahead of the geometric throat, but this was not altered during the experiment.

In the forward centerbody interaction region, 20° slanted holes of 0.159-cm minor axis and a scoop of height 0.127 cm were the bleed configurations used. The aft centerbody bleed consisted of 0.318-cm diameter holes normal to the surface (Fig. 3a). The three different bleed sections used in the cowl interaction region (Fig. 3b) were: 1) 0.318-cm diameter normal holes; 2) 0.159-cm diameter normal holes; and 3) 0.318-cm minor axis holes slanted at 20° to the surface. The cowl bleed sections were termed large normal (LN), small normal (SN), and slant for the respective bleed regions. More detailed information on the bleed region geometry may be found in Ref. 9.

The effect of bleed location, relative to the shock-induced pressure-rise, on the boundary layer was investigated by opening or closing rows of holes. The three general bleed hole patterns used were rows of holes open upstream of the shock reflection (US), holes open downstream of the shock reflection (DS), and holes open across the shock reflection (AS).

The amount of bleed mass flow was also controlled during the experiment. Pipes with calibrated exit plugs were fitted over the bleed exit passages on the cowl and bleed mass flow was controlled by remotely actuating the exit plugs.

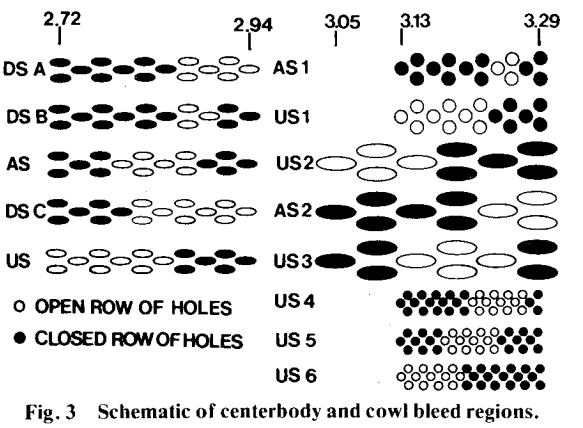

Fig. 3 Schematic of centerbody and cowl bleed regions.

Pressure Measurements

Static pressure measurements were made on cowl and centerbody surfaces, mainly on the bottom centerline. The static taps in the bleed regions were staggered around the bottom centerline to minimize interference effects.

Boundary-layer total pressure profiles were measured before and after the shock/boundary-layer interactions with a total of seven traversing Pitot tubes. These Pitot tubes had flattened tips and an inner height of 0.010 cm, an outer height of 0.020 cm, and a width of 0.096 cm. Two surface static pressure measurements were also made at the probe tip location. The probes and their locations relative to the shock impingement points are shown in Fig. 2. Compressor-face total pressure measurements were also made.

The assumptions made in the calculation of velocity data from Pitot tube data were: 1) a Crocco temperature profile with Prandtl number equal to one; and 2) a negligible normal pressure gradient at the probe tip location.

Test Procedure

The experiment was conducted with a test section Mach number of 2.50 and data were taken at unit Reynolds numbers of 8.2 and 5.75×10^6 per meter, although only the data for the higher Reynolds number will be presented. The inlet was operated in two modes of terminal shock position. In the supercritical mode the terminal shock was positioned downstream of the geometric throat, while in the critical mode the terminal shock was held at the geometric throat. Most of the data were taken in the supercritical mode because the terminal shock was much more stable in this mode at low bleed rates. The testing procedure was to obtain maximum mass flow through the bleed regions once the inlet was at the design Mach number. Then the centerbody bleed mass flow was reduced and the data were taken. The centerbody bleed mass flow was then increased and the same procedure was followed with the cowl bleed mass flow.

The boundary layers at the initial Pitot probe locations on the centerbody and cowl were turbulent and no artificial means to trip the boundary layers was used.

Results

Centerbody Shock/Boundary-Layer Interactions

The inlet was operated in the supercritical mode, with the terminal shock held downstream of the geometric throat, for much of the experiment and only the first two centerbody interactions were investigated. The boundary layer on the centerbody was surveyed before and after each of the interactions by Probes 1 to 4 at x/R_c locations of 2.685, 3.039, 3.303, and 3.557, respectively. The shock impingement points, as calculated by the method of Ref. 10, were at respective x/R_c values of 2.88 and 3.48 for the two interactions, and a comparison of the experimental and calculated pressure distribution is shown in Fig. 4. There was little change in shape of the static pressure distributions for the various centerbody bleed regions, so only a representative sample is shown.

The bleed hole configurations used in the forward centerbody bleed section are those presented in Fig. 3a. There were several different downstream (DS) bleed configurations used in the forward centerbody, labelled DS A, DS B, and DS C, while only single across-shock (AS), upstream (US), and scoop bleed configurations were tested.

The boundary layer at Probe 1, ahead of the first centerbody interaction region, had an edge Mach number of 2.09 and the wall temperature of 297°K was very close to the adiabatic wall temperature. The transformed form factor, H_{tr}, was 1.26 with compressible displacement and momentum thicknesses, δ^* and θ, of 0.096 cm and 0.030 cm, respectively. The data at Probe 1 varied less than 5% from the values of H_{tr}, δ^*, and θ presented.

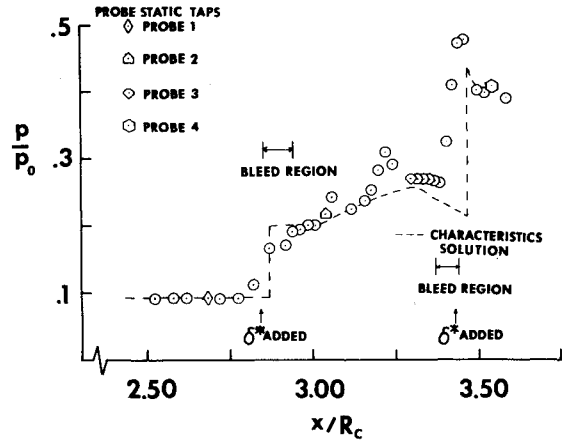

Fig. 4 Comparison of centerbody static pressure distribution with the method of characteristics computation.

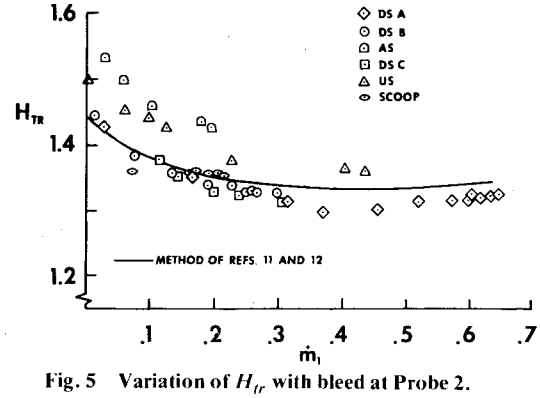

Fig. 5 Variation of H_{tr} with bleed at Probe 2.

The variation of H_{tr} with nondimensional bleed mass flow at Probe 2, which was behind the first interaction region, is presented in Fig. 5. The nondimensional bleed mass flow, $\dot{m}_I$, was defined as the bleed mass flow in the forward centerbody bleed section divided by the Probe 1 boundary-layer mass flow. The Probe 1 boundary-layer mass flow was 1.87% of the inlet-capture mass flow. The average wall temperature at Probe 2 was 300.7°K and the average Mach number was 1.63. The edge Mach number and wall temperature showed slight increases with increasing bleed mass flow.

To compare with experimental results, boundary-layer parameters were calculated. The integral model of Sasman and Cresci[11] was used to calculate turbulent boundary-layer growth before and after the interaction, with the Seebaugh, Paynter, and Childs[12] scoop bleed model used to compute the boundary-layer growth across the interaction region. The assumptions made and the general applicability of the scoop bleed model are enumerated in Ref. 14. At Probe 1 the calculations yielded H_{tr}, δ^*, and θ of 1.30, 0.134 cm, and 0.0381 cm, respectively; these values were higher than those obtained experimentally.

The transformed form factor at Probe 2 (Fig. 5) varied smoothly for all bleed configurations tested and, in most cases, asymptotically reached a minimum value. This plateau in H_{tr} was generally reached at a bleed mass flow of 30% to 40% of the Probe 1 boundary-layer mass flow, but values of the plateau form factors for the different bleed regions were not necessarily the same. The velocity profiles at Probe 2, shown in Fig. 6 for various bleed rates, showed very little change in shape for $\dot{m}_I$ greater than 0.3 but became progressively less full for smaller bleed rates. This trend was reflected in the transformed form factor, as the H_{tr} for an $\dot{m}_I$ of 0.60 was 1.32 while the H_{tr} for an $\dot{m}_I$ of 0.025 was 1.43. Since no significant decrease in H_{tr} was obtained for bleed mass flows greater than 35% of the Probe 1 boundary layer mass flow, more bleed could be considered unnecessary.

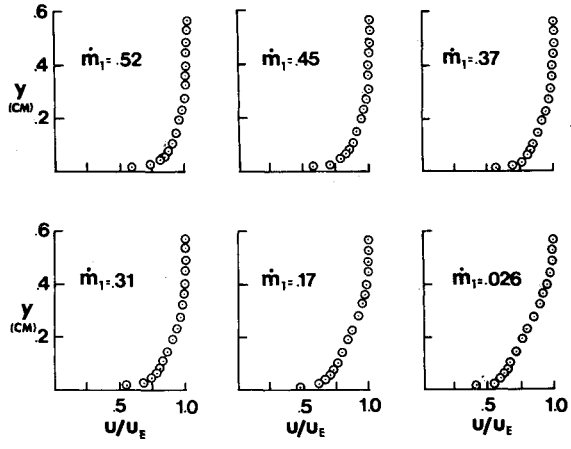

Fig. 6 Velocity profiles for varying bleed Rates at Probe 2.

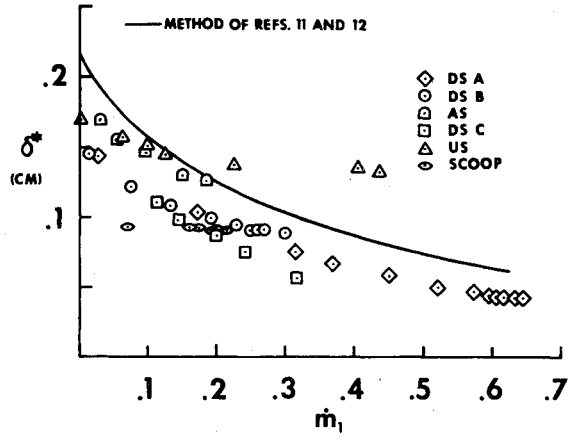

Fig. 7 Varition of δ^* with bleed at Probe 2.

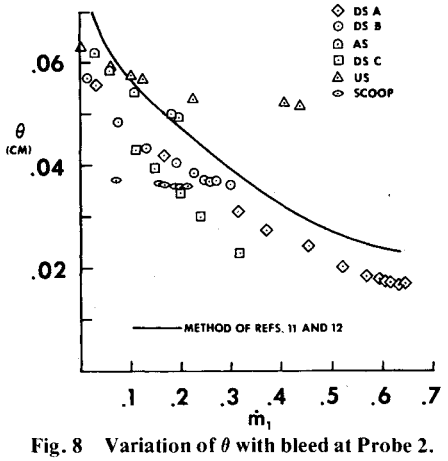

Fig. 8 Variation of θ with bleed at Probe 2.

In general, the DS bleed configurations provided the lowest form factors for a given bleed rate, with the US and AS bleed regions respectively higher. The data for the DS bleed regions show very little effect of the different bleed configurations used except that more bleed mass flow was obtained when more bleed holes were opened. The consistently largest form factors for a given bleed rate were obtained while using the AS bleed configuration. Static pressure measurements showed that the bleed region spanned the shock-induced pressure rise; thus some amount of recirculation may have been present, as all the bleed holes vented into a single plenum. The scoop bleed configurations showed almost no change in transformed form factor; however, only a small range of bleed mass flows was obtained. The scoop was placed in the middle of the shock interaction region, $x/R_c = 2.84$, and seemed to minimize upstream propagation of the higher pressure behind the shock waves. A comparison of the calculated form factors to the experimental data shows good agreement in that the calculations reliably follow the trends in the data. The shock/boundary-layer interaction model does not differentiate between bleed regions relative to the shock-induced pressure rise, so only a single curve was obtained for H_{tr} as a function of bleed mass flow. An interesting point to note about the calculated form factor curve was the slight increase in form factor predicted for bleed mass flows, $\dot{m}_1$, greater than 0.35.

An extrapolation of the data to zero bleed showed that the different bleed configurations had unequal transformed form factors, displacement, and momentum thicknesses at Probe 2. This was probably due to roughness effects and possible recirculation via the bleed plenum between Probes 1 and 2. In a previous investigation using the same inlet and test conditions except that a solid wall was present between Probes 1 and 2, the transformed form factors were 1.28 at Probe 1 and 1.48 at Probe 2. In this investigation, the extrapolated zero bleed form factors at Probe 2 for the DS, US, and AS bleed configurations were approximately 1.43, 1.50, and 1.55, respectively.

The variation of δ^* and θ at Probe 2 are presented in Figs. 7 and 8. These data show the same trends as the form factor data in that the AS and US bleed configurations had the largest values and the three DS configurations were grouped at lower values. The data show that δ^* and θ were still decreasing at the larger bleed mass flow rates; however, the ratio of these parameters, the compressible form factor, remained constant. The ranges of δ^* and θ were 0.17 cm to 0.04 cm and 0.065 cm to 0.018 cm, respectively, for bleed rates, $\dot{m}$, from 0.2% to 65%; while at Probe 1, δ^* and θ were 0.096 cm and 0.030 cm, respectively. A comparison of the calculated and experimentally obtained values shows that the models used predicted larger values of δ^* and θ than were obtained from the test. The model accurately predicts the behavior of a majority of the DS bleed data but seems to underestimate the effect of the bleed.

The results at Probe 2 indicate that the DS bleed configuration gave the lowest values of H_{tr}, δ^*, and θ. However, the data at Probe 2 were influenced to some extent by the closeness of the probe location to the interaction and bleed regions. In order to examine this point in more detail, the data at Probe 3, $x/R_c = 3.303$, have been analyzed to see if the effects observed at Probe 2 persisted downstream.

The variation of H_{tr} with $\dot{m}_1$ at Probe 3 is presented in Fig. 9. The transformed form factors obtained at Probe 3 were always lower than those at Probe 2 for a given bleed region geometry and bleed mass flow rate. The primary effect on the reduction in H_{tr} seemed to be the 'recovery' of the boundary layer after the shock interaction region. Growth of the boundary layer is very rapid through the shock interaction region but cannot be sustained once out of the interaction region, and a reduction in H_{tr} then occurs. A secondary cause of the reduction in boundary-layer growth was then the existence of a slight favorable pressure gradient ahead of Probe 3.

The data at Probe 3 show that US and DS C bleed configurations had the lowest form factors and, in general, there was much less variation in H_{tr} at Probe 3 than at Probe 2. The H_{tr} data all fell in the range from 1.30 to 1.55. These data indicate that the results obtained at Probe 2, slightly downstream of the interaction, exhibited some local effect of bleed in the interaction region and that a physical smoothing out process occurs downstream which decreases the sensitivity of the boundary layer to the local bleed geometry in the first interaction region. The comparison between the experimental data and the calculations again showed that the calculated form factors were larger than those observed; however, the reduction in H_{tr} for all bleed rates in going from Probe 2 to Probe 3 was predicted by the model.

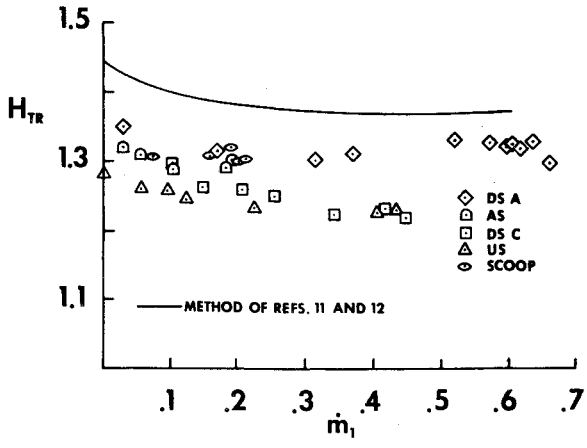

Fig. 9 Variation of H_{tr} with bleed at Probe 3.

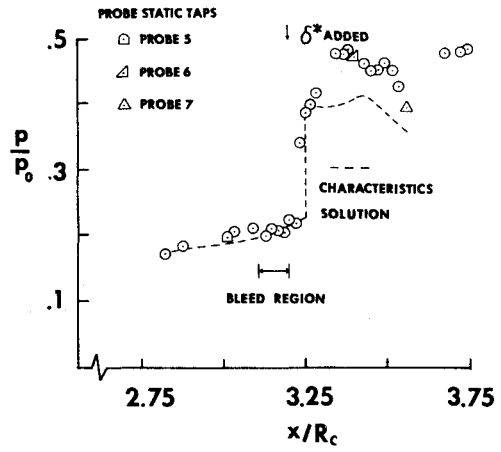

Fig. 10 Comparison of cowl static pressure distribution with the method of characteristics computation.

A significant amount of bleed, 0.8% to 2.3% of the inlet's capture mass flow, was used in the second centerbody interaction region. As a result of bleeding in two different regions and the variable nature of the boundary layer entering the second centerbody interaction region, the data at Probe 4, $x/R_c = 3.557$, were somewhat scattered. However, all the transformed form factors at Probe 4 lay between 1.33 and 1.43. The low values for H_{tr} obtained at Probe 4 were due to the large amounts of bleed used and because the terminal shock had not been encountered as the flow was still supersonic at Probe 4.

The amount of error in the values of H_{tr} obtained at Probes 1, 2, and 3 was estimated to be no more than 8% when the bleed rates were less than 50% of the Probe 1 boundary-layer mass flow.

Cowl Interaction Region

The cowl boundary layer was surveyed before the interaction region by Probe 5 at $x/R_c = 3.006$ and after the interaction by Probes 6 and 7 at $x/R_c = 3.394$ and 3.557, respectively. The first shock impingement point calculated by the method of Ref. 10 was at $x/R_c = 3.25$, while the δ^*-added method predicted a shock impingement point at $x/R_c = 3.20$.

The boundary layer at Probe 5 had H_{tr}, δ^*, and θ of 1.34, 0.061 cm, and 0.023 cm, respectively. The edge Mach number was 1.66 and the wall temperature of 307°K was very close to the adiabatic wall temperature. The boundary-layer mass flow at Probe 5 corresponded to 3.6% of the inlet's capture mass flow. The data at Probe 5 also varied less than 5% for all of the data presented.

A stronger shock wave than anticipated was encountered on the cowl and is shown in Fig. 10 along with the calculated pressure distribution. Due to the larger pressure rise across the interaction region on the cowl than on the centerbody, inlet unstart was a prominent danger. In addition, the shock impingement point appeared to be downstream of the bleed region with a larger shock pressure rise than predicted theroetically. As a result, most of the bleed regions tested were upstream of the shock-induced pressure rise and only two AS bleed regions were used.

The variation of H_{tr} at Probe 6, behind the interaction region, with bleed mass flow is presented in Fig. 11. The nondimensional bleed mass flow $\dot{m}_5$ is defined as the cowl bleed mass flow divided by the boundary-layer mass flow at Probe 5. The average edge Mach number at Probe 6 was 1.05, with T_W being 307°K. In Fig. 11, only representative examples of the different types of bleed regions have been shown as all of the data examined showed only small differences for similar bleed region geometries.

A comparison of the data at Probe 6 show that the AS 1 large-normal-hole bleed region had the largest form factors, greater than 1.68 for all bleed mass flows. These large form factors imply that unstart may occur at these bleed rates in

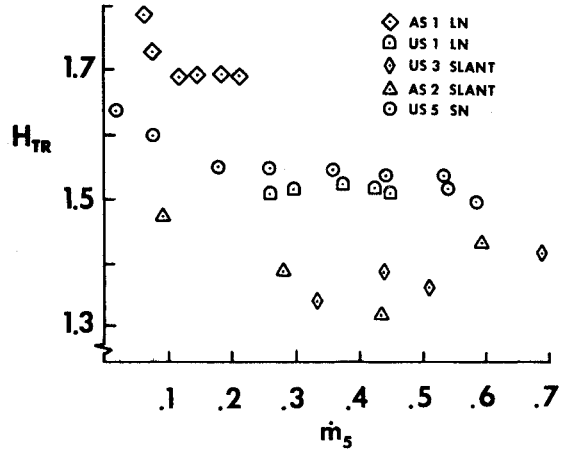

Fig. 11 Variation of H_{tr} with bleed at Probe 6.

critical operation, and unstart did occur in supercritical operation with $\dot{m}_5$ less than 7% for this bleed configuration.

The lowest form factors were obtained with the slanted-hole bleed regions. The effect of bleed region geometry can be isolated by comparing the data for bleed regions US 3 slanted and US 4 small normal as they were placed in similar locations. Plateau transformed form factors of 1.3-1.4 were obtained with the slanted-hole bleed regions while plateau form factors of 1.55 were obtained with the normal-hole bleed regions. The plateau transformed form factors for each of the bleed regions were obtained with $\dot{m}_5$ less than 40%.

The effect of hole size, comparing the normal-hole bleed regions US 1 and US 5, showed that a slightly smaller H_{tr} was obtained with the smaller holes, but the difference did not seem significant.

In general, the plateau transformed form factors obtained were 1.35 for the slanted-hole bleed regions, 1.52 for the US normal-hole bleed regions, and 1.68 for the AS normal-hole bleed region.

The AS 2 slanted-hole bleed data seemed to present an anomaly in that the form factors obtained at Probe 6 were approximately the same as those obtained with the US 3 slanted-hole bleed region. However, an examination of the static pressure distributions showed that the pressure gradient along the AS 1 normal-hole bleed region was more than four times greater than that along the AS 2 slanted-hole bleed region, while the pressure gradients along the slanted-hole bleed regions, AS and US, were comparable. So the possibility of recirculation was much less with the slanted-hole, compared to the normal-hole, bleed region in the AS bleed configuration. Thus, the performance of the bleed region seems

to be dependent on the pressure gradient along the bleed region.

Althought not presented graphically, the average values of δ^* and θ for $\dot{m}_5$ greater than 15% were 0.15 cm and 0.066 cm, respectively, for the AS 1 normal-hole bleed region, while for the US normal-hole bleed region the values were 0.097 cm and 0.047 cm, respectively. The values of δ^* and θ for the slanted-hole bleed regions continually decreased for increasing bleed rates. For values of $\dot{m}_5$ greater than 15%, the values of δ^* and θ were less than 0.13 cm and 0.96 cm, respectively.

Calculations of boundary-layer parameters through the shock interaction region were attempted, but the method of Ref. 12 yielded no solution for the experimental pressure distributions and bleed mass flow rates used.

The data at Probe 7, $x/R_c = 3.55$, although not presented graphically, showed the same trends observed on the centerbody, namely that there was an observed decrease in H_{tr}, δ^*, and θ when compared to the data directly behind the interaction region. Probe 7 was slightly downstream of the geometric throat and because of supercritical operation the flow was still supersonic with no interaction region between Probes 6 and 7. All of the data on H_{tr} were in the range form 1.23 to 1.36 at Probe 7. So, the effects of bleed region geometry were not significant far downstream of the interaction region as was seen on the centerbody. However, the normal-hole AS bleed region had transformed form factors slightly larger than other bleed regions tested at this location. The average edge Mach number at Probe 7 was 1.23, with T_w being 300°K.

Pressure Recovery

Although most data were taken in supercritical operation, with compressor-face pressure recoveries on the order of 78%, some data were obtained for critical operation. The highest compressor-face total pressure recovery obtained was 89.9%, with a distortion level of 10.3% and a bleed mass flow of 4.7% of the capture mass flow. The lowest compressor-face total pressure recovery obtained was 89.2%, with a distortion level of 11.1% and a bleed mass flow of 3.1% of the capture mass flow. In comparison, other experiments[15] on basically the same inlet have yielded compressor-face total pressure recoveries of 92%, with a bleed rate of 10% of the capture mass flow rate.

Conclusions

An experimental investigation was conducted to determine the effect of bleed on a boundary layer after a shock-wave/boundary-layer interaction in an axisymmetric, mixed compression supersonic inlet. The effects of bleed amount and bleed region geometry on the boundary layer after a shock/boundary-layer interaction region have been presented.

The results show that the transformed form factor, H_{tr}, directly after an interaction region decreases with increasing bleed until a plateau is reached. The level of the plateau was found to be dependent on the placement of the bleed region relative to the shock-induced-pressure rise. The plateau transformed form factors were usually reached within bleed mass flows of 45% of the boundary-layer mass flow before the interaction region and the larger bleed mass flows are unnecessary. The effectiveness of bleed for smaller mass flows was dependent on bleed region location and geometry.

A comparison of bleed configurations showed that the AS bleed configuration, open rows of holes spanning the shock-induced pressure gradient, generally had the largest transformed form factors and thicknesses. The relatively large boundary-layer parameters may have been due to recirculation in the bleed region. For the inlet geometry of this investigation, the AS type of bleed region should be avoided.

Acceptable transformed form factors for critical inlet operation were obtained with the US, DS, and scoop bleed configurations. At larger bleed mass flow rates, the DS bleed configurations provided the lowest form factors directly behind the bleed region, while farther downstream of the interaction the US bleed configurations had slightly lower form factors. This suggests that the lower values of H_{tr} obtained with the DS bleed configurations was a local effect and that there is not enough overall difference between the US and DS bleed to prefer one over the other with regards to H_{tr}.

The results comparing the effects of normal- and slanted-hole bleed regions on the cowl showed that the slanted-hole bleed sections were much more effective in providing lower form factors directly behind the interaction region. However, only slight differences were obtained farther downstream between normal- and slanted-hole bleed sections. The results comparing the effects of 0.159-cm and 0.318-cm diameter normal bleed holes on the cowl showed that there was no discernible effect of bleed hole size on the boundary layer after the interaction region.

Acknowledgment

This work was supported by NASA Lewis Research Center under grant NGR-36-027-038 (Graduate Research Program in Aeronautics).

References

[1] Cubbison, R.W., Meleason, E.T., and Johnson, D.F., "Effect of Porous Bleed in a High Performance Axisymmetric Mixed Compression Inlet at Mach 2.50," NASA TM X-1692, 1968.

[2] Hingst, W.R. and Johnson, D.F., "Experimental Investigation of Boundary Layers in an Axisymmetric, Mach 2.5, Mixed Compression Inlet," NASA TM X-2902, 1973.

[3] Smeltzer, D.B. and Sorensen, N.E., "Analytical and Experimental Performance of Two Isentropic Mixed Compression Axisymmetric Inlets at Mach Numbers 0.8 to 2.5," NASA TN D-7320, 1973.

[4] Kilburg, R.F.and Kotansky, D.R., "Experimental Investigation of a Plane, Oblique Incident-Reflecting Shock Wave with a Turbulent Boundary Layer on a Cooled Surface," NASA CR-66841, 1969

[5] Strike, W.T. and Rippey, J.O., "Influence of Suction on the Interaction of an Oblique Shock with a Turbulent Boundary Layer at Mach 3.0," Arnold Engineering Development Center, Tullahoma, Tenn., Rept. AEDC-TN-61-129, 1961.

[6] McLafferty, G. and Ranard, E., "Pressure Losses and Flow Coefficients of Slanted Perforations Discharging from within a Simulated Supersonic Inlet," United Aircraft Corp., East Hartford, Conn., UAC R-0920-01, 1958.

[7] Smeltzer, D.B.and Sorenson, N.E., "Performance Estimates for a Supersonic Axisymmetric Inlet System", *Journal of Aircraft,* Vol. 9, Oct. 1972, pp. 703-706.

[8] Syberg, J. and Koncsek, J.L., "Bleed System Design Technology for Supersonic Inlets," *Journal of Aircraft,* Vol. 10, July 1973, pp. 407-413.

[9] Fukuda, M.K., Hingst, W.R., and Reshotko, E., "Control of Shock Wave-Boundary Layer Interactions by Bleed in Supersonic Mixed Compression Inlets," NASA CR-2595, 1975.

[10] Anderson, B.H., "Design of Supersonic Inlets by a Computer Program Incorporating Method of Characteristics," NASA TN D-4960, 1969.

[11] Sasman, P.K. and Cresci, R.J., "Compressible Turbulent Boundary Layers with Arbitrary Pressure Gradient and Heat Tranfer," *AIAA Journal,* Vol. 9, Jan. 1966, pp. 19-25.

[12] Seebaugh, W.R., Paynter, G.C., and Childs, M.E., "Calculation of Turbulent Boundary Layer Characteristics Across an Oblique Shock Reflection Including the Effects of Mass Bleed," *Journal of Aircraft,* Vol. 5, Sept.-Oct. 1968, pp. 461-467.

[13] Sorenson, V.L., "Computer Program for Calculating Flow Fields in Supersonic Inlets," NASA TN D-2897 1965.

[14] Hingst, W.R. and Towne, C., "Comparison of Theoretical and Experimental Boundary Layer Development in a Mach 2.5 Mixed, Compression Inlet," NASA TM – X-3026, 1974.

[15] Cubbison, R.W., Meleason, E.T., and Johnson, D.F., "Performance Characteristics from a Mach Number of 2.58 to 1.98 of a Axisymmetric Mixed Compression Inlet System with 60 Percent Internal Contraction," TM X-1739, 1969.